Supplementary information

Targeting temporal dynamics of microenvironmental factors halts tumor migration and alleviates effects of tumor heterogeneity

Manjulata Singh[1, #], Xiao-Jun Tian[2, [+], #], Vera S. Donnenberg[1,3], Alan M Watson[4], Jingyu Zhang[2], Laura P. Stabile[5], Simon C. Watkins[6], Jianhua Xing[2, 7 *], Shilpa Sant[1, 8 *]

[1] Department of Pharmaceutical Sciences, School of Pharmacy, University of Pittsburgh, PA, USA
[2] Department of Computational and Systems Biology, School of Medicine, University of Pittsburgh, PA, USA
[3] Department of Cardiothoracic Surgery, University of Pittsburgh School of Medicine, McGowan Institute for Regenerative Medicine, and UPMC-Hillman Cancer Center, University of Pittsburgh, Pittsburgh, PA, USA
[4] Center for Biologic Imaging, Center for Vaccine Research, and Department of Immunology
University of Pittsburgh, Pittsburgh, PA, USA
[5] Department of Pharmacology & Chemical Biology, UPMC-Hillman Cancer Center, Pittsburgh, PA, USA
[6] Center for Biologic Imaging and the Department of Cellular Biology, University of Pittsburgh, Pittsburgh, PA, USA
[7] UPMC-Hillman Cancer Center, University of Pittsburgh, Pittsburgh, PA, USA
[8] Department of Bioengineering, Swanson School of Engineering, McGowan Institute for Regenerative Medicine, and UPMC-Hillman Cancer Center, University of Pittsburgh, Pittsburgh, PA, USA
[+] Current Address: School of Biological and Health Systems Engineering, Arizona State University, Tempe, AZ, USA

[#]These authors contributed equally to this work.

Corresponding Authors:

Shilpa Sant, PhD
Email: shs149@pitt.edu
Phone: +1 4126489804
Address: 808A Salk Hall, 3501 Terrace Street, Pittsburgh, PA, 15261 USA.

Jianhua Xing, PhD
Email: xing1@pitt.edu
Phone: +1 4123835743
Address: Suite 3084, Biomedical Science Tower 3 (BST3), 3501 Fifth Avenue, Pittsburgh, PA, 15261 USA.

Material and Methods

Microtumor fabrication from patient-derived primary metastatic breast cancer and mesothelioma cells

Metastatic breast cancer (mBC) cells were cultured using mammary epithelial growth media (MEGM) with 10 % FBS and 0.1% penicillin-streptomycin in T175 flask till they become 50% confluent. Mesothelioma cells were cultured in DMEM containing with 10% FBS, 2.0 mM L-Glutamine and 0.1% penicillin-streptomycin in tissue culture flask until 40-60% confluent. Cells were trypsinized, counted and seeded on 1x1 cm^2 PEGDMA hydrogel microwell arrays (150 and 600 μm) at a density of 0.5 and 1.0 million cells per device for mBC and mesothelioma cells, respectively as described for microtumor fabrication from cancer cell lines. The microtumors were cultured up to 6 to7 days. Both 150 and 600 μm microtumors were harvested on day 6 (mesothelioma) and day 7 (mBC). Media were collected to measure the levels of FN and sE-CAD.

Establishment of patient-derived xenografts (PDX)

For initial PDX establishment (F1), two 2 mm^2 pieces of tumor tissue from a non-small cell lung cancer (NSCLC) PDX model established from a brain metastasis (BM012-15) were implanted subcutaneously in the hind flanks of 6-week old NOD.Cg-Prkdc Il2rg/SzJ (NOD scid gamma) mice. PDX tumors were allowed to grow until a size of more than 500 mm^3 followed by removal for serial transplantation to the next generation (F2). Once the tumor size reached 500 mm^3 in the F4 generation, the PDX was removed for preparation of the PDX cell suspension. The BM012-15 PDX model harbored the *KRAS* G12C mutation and was derived from an ex-smoker.

Preparation of PDX cell suspension

Finely minced PDX tissue was disaggregated using collagenase (41 U/mL) and hyaluronidase (100 U/ml) at 37°C under constant rotation for 40-50 min. Disaggregated tumor slurry was passed through 70 μm cell strainer to remove the undissociated or large tissue pieces. Single cells suspension was obtained by digesting the strained cells with 0.25% Trypsin for 5-10 min at 37°C and centrifuging them at 500 x g for 5 min. Cell number and viability was determined by trypan exclusion method. Cells were seeded in flask at cell density of 30,000 cells/cm^2 using RPMI media with 10% FBS and 0.1% penicillin-streptomycin and allowed to adhere for 48 h. The viability was assessed by live-dead assay (Calcein-AM and ethidium homodimer) after 24 h in a separately seeded culture dish.

Fabrication of PDX cell microtumors

After 48 h, the cells in the flask had adhered fibroblast like cells and multiple floating aggregates of cancer cells. The floating aggregates were collected and disaggregated by vigorous pipetting. Cells were counted and seeded on 1x1 cm^2 hydrogel device (150 and 600 μm well size) at a density of 0.5 million cells/device and cultured up to 8 days in incubator at 37°C and at 5% CO_2. Fifty percent media was changed every day and the microtumors were monitored for their migratory behavior. Microtumors were harvested on day 8 and media were collected to measure the levels of FN and sE-CAD.

Description of gene regulatory network

In our previous study, we found that the migratory phenotype of 600 μm microtumors is irreversible even after reversing its size to 150 μm (Singh et al., 2016). Furthermore, we

found that HIF-1α knockdown only partially downregulates mesenchymal markers. However, the underlying molecular mechanism of these interesting phenomena is not clear. In this study, we found that the microtumor size-associated microenvironmental changes including HIF-1α, MMP9 and sE-CAD are critical for the migration ability of the microtumor. Combining this information with our previous work and interactions among these regulators and Epithelial-mesenchymal transition regulators, we first obtained an integrated regulatory network as shown in **Fig. S3**. HIF-1α is stabilized by the hypoxia, which is caused by the increase in the microtumor size. HIF-1α increases the expression of MMP9 (Choi et al., 2011). MMP9 functions as a protease that cleavage E-Cadherin (E-CAD) and generate soluble sE-CAD (De Wever et al., 2007; Maretzky et al., 2005). sE-CAD is able to induce the activation of EGFR/ERK signaling pathway (Brouxhon et al., 2014; Inge et al., 2011; Moshal et al., 2006; Patil et al., 2015; Zuo et al., 2011). Moreover, FN (Fibronectin) and pro-MMP9 are downstream of EGFR/ERK (Jeon et al., 2015). The activation of MMP9 from its pro-form is mediated by FN (Das et al., 2008; Mitra et al., 2006; Sen et al., 2010). Thus, the activation of MMP9 by FN and ERK pathway are dependent. One of the common downstream targets of the HIF1-α and ERK is SNAIL1 (Evans et al., 2007; Luo et al., 2011; Zhang et al., 2013), which together with TWIST1, functions as the core regulator of the epithelial to mesenchymal transition by increasing the expression of Vimentin (VIM) and E-CAD. However, in our experiments, no change was found in the protein expression of E-CAD (**Fig. 1G**) and as reported previously by Lundgren et al (Lundgren et al., 2009). Also, the nuclear level of SNAIL1 in hypoxia-treated T47D was low (Lundgren et al., 2009). Based on this information and for simplicity, in this work, we focus more on the secretome of the microtumor and the molecular mechanism of migration regulated by the secretome molecules. Thus, we

simplified the network to a minimal model with only the key nodes such as HIF-1α, MMP9, sE-CAD and FN, and we built a mathematical model as following (**Fig. 4A-B**).

Gompertz growth model is used for micro-tumor growth

$$\text{Tumor size} = \text{Tumor size}_{\max} * \left(\frac{\text{Tumor size}_0}{\text{Tumor size}_{\max}}\right)^{\exp(-\alpha * t)}$$

Where $\text{Tumor size}_{\max}$ is the carrying capacity of the microwell, which controls the maximum size of the microtumor. Tumorsize_0 is the initial size of the microtumor after seeding. We use two sizes of microwells (150 μm and 600 μm) in our experiments. α is a growth constant related to the proliferation rate of the tumor cells.

The following ODEs are used for bifurcation analysis.

$$\frac{d[\text{HIF1}\alpha]}{dt} = k_{\text{HIF1}} - d_{\text{HIF1}} * [\text{HIF1}\alpha] * \frac{1}{1 + \frac{\text{Tumor size}}{J_{\text{HIF1}}}}$$

$$\frac{d[\text{MMP9}]}{dt} = k1_{\text{MMP}} * [\text{HIF1}\alpha] + k2_{\text{MMP}} * [\text{FN}] - d_{\text{MMP}} * [\text{MMP9}]$$

$$\frac{d[\text{sEcad}]}{dt} = k_{\text{sEcad}} * \text{Ecad} * [\text{MMP9}] - d_{\text{sEcad}} * [\text{sEcad}]$$

$$\frac{d[\text{FN}]}{dt} = k_{\text{FN}} * \frac{[\text{sEcad}]^2}{[\text{sEcad}]^2 + J_{\text{FN}}^2} - d_{\text{FN}} * [\text{FN}]$$

Here, [HIF1] is the total level of HIF-1α for total microtumor, while [MMP], [sEcad] and [FN] are the total levels of MMPs, soluble E-CAD and FN in the microenvironment (conditioned media, CM). A constant level of E-CAD is used in the model since no significant change of E-CAD is found in the experiment (**Fig. 1G**). It is noted the

heterogeneity of the microtumor is considered explicitly, such as a variance of the growth variability (α), the Michaelis constant of tumor size, hypoxia-mediated inhibition of HIF1α degradation J_{HIF1} and the initial cell seeding number. The parameter value of α and J_{HIF1} is randomly chosen from 80 to 120% of its default value. The initial diameter of 150 μm microtumors are 82±33 while that of 600 μm are 394±46 (Singh et al., 2016) as measured in our previous work (Singh et al., 2016). It is noted that our model focuses on the interaction between the microtumor cells and the microenvironmental factors and single microtumor fate. We use the level of soluble E-CAD, [sE-CAD], in the microenvironment as the readout of the model to represent the migratory fate of the microtumor.

Supplementary Table 1. List of primers used

No.	Name	Sequence
1.	MMP9 - Forward	5’-GGTGATTGACGACGCCTTTG-3’
	MMP9 - Reverse	5’-GGACCACAACTCGTCATCGT-3’
2.	Vimentin - Forward	5’-CAA CCT GGC CGA GGA CAT-3’
	Vimentin - Reverse	5’-ACG CAT TGT CAA CAT CCT GTC T-3’
3.	Fibronectin -Forward	5’-CCG CCG AAT GTA GGA CAA GA-3’
	Fibronectin - Reverse	5’-TGC CAA CAG GAT GAC ATG AAA-3’
4.	E-cadherin - Forward	5’- GAA CAG CAC GTC CAC AGC CCT-3’
	E-cadherin - Reverse	5’- GCA GAA GTGTCC CTG TTC CAG-3’
5.	β-actin - Forward	5’-ACC TTCTAC AAT GAG CTG CG-3’
	β-actin - Reverse	5’CCT GGA TAG CAA CGT ACA TGG-3’

Supplementary Table 2. Parameters used in the ODEs

Parameter	Description	Value
α	Growth rate of micro-tumor	13
k_{HIF1}	The expression rate of HIF-1α	10
d_{HIF1}	The degradation rate of HIF-1α	20
J_{HIF1}	Michaelis constant of tumor size/Hypoxia-mediated inhibition of HIF1α degradation	732
$k1_{MMP}$	The secretion rate of MMP mediated by HIF-1α	8
$k2_{MMP}$	The secretion rate of MMP mediated by FN	55
d_{MMP}	Degradation rate of MMP	50
k_{sEcad}	The production rate of soluble E-CADHERIN	16.5
d_{sEcad}	Degradation rate of soluble E-CADHERIN	11
k_{FN}	The production rate of FN	50
d_{FN}	Degradation rate of FN	25
J_{FN}	Michaelis constant of s-ECAD mediated production of FN	1.6

Fig. S1

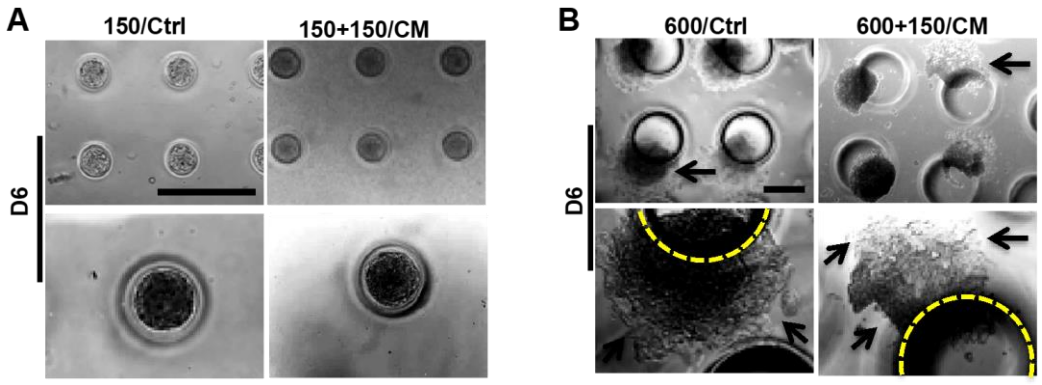

Supplementary Figure S1: Treatment of 150 and 600 μm microtumors with conditioned media of 150 μm microtumors (150/CM). To test the effect 150 μm microtumor secretome on collective migration, both 150 and 600 μm microtumors were treated with 150/CM. (A) Photomicrographs showing no migration in 150 μm microtumors treated with 150/CM; (B) 600 μm microtumors treated with 150/CM showed migratory pattern similar to control (untreated) 600 μm microtumors. Images represent the data of two independent experiments with at least 3 devices containing multiple microtumors in each experiment. Scale bar: 500 μm.

Fig. S2

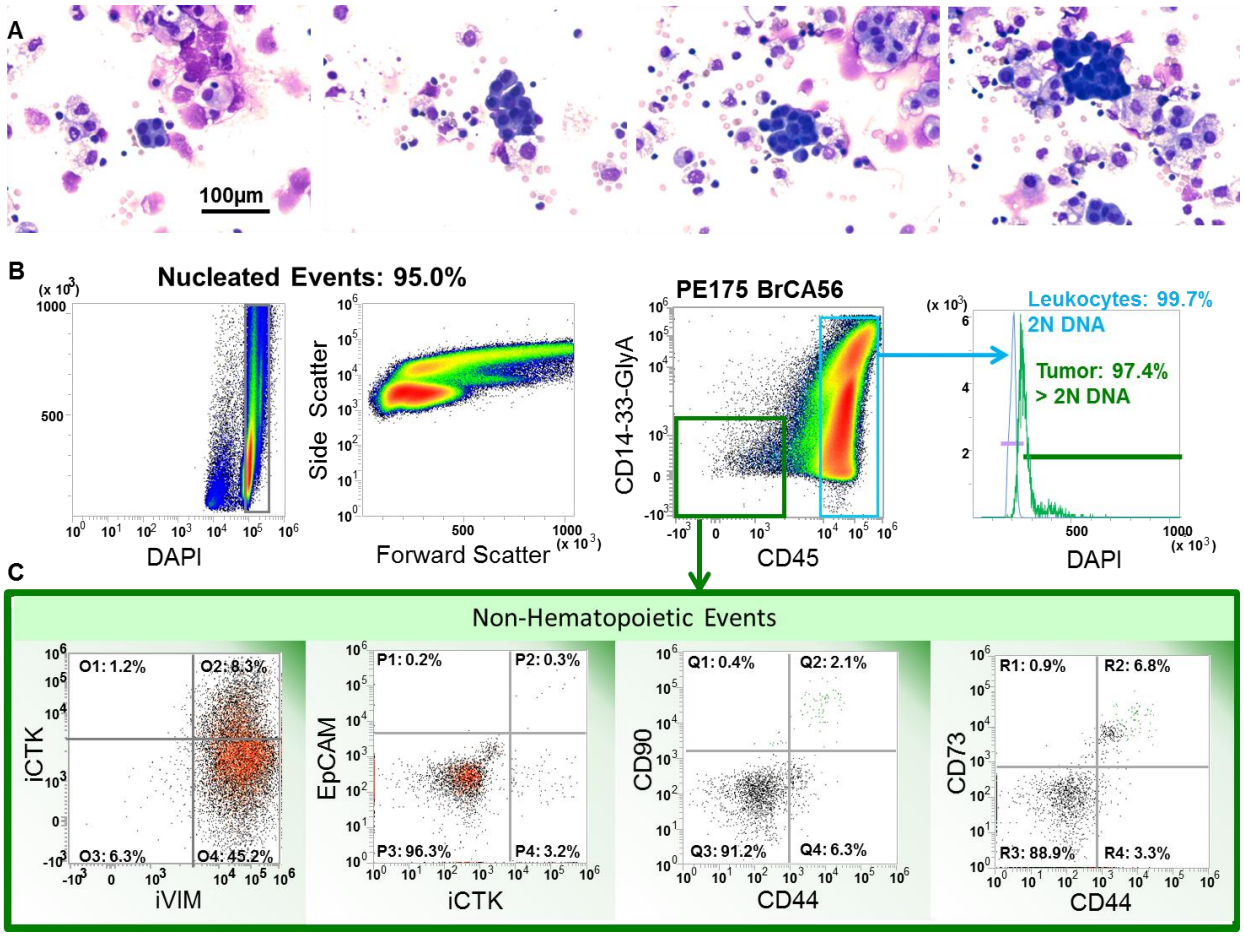

Supplementary Figure S2: Morphology and multi-parameter flow cytometry on breast cancer metastatic pleural effusion cells. Photomicrographs of cytocentrifuge preparations of malignant pleural effusion (metastatic breast cancer, MPE175) used in this study are shown (Panels A, top row). Phase contrast images were photographed using a 10X objective and are unmodified. A Nikon Diaphot microscope equipped with a Spot Insight camera was used. Despite the metastatic, highly invasive and mostly EMT nature of malignant pleural effusions, only microtumor clusters are detectable (< 150 µm). Flow cytometric analysis of the freshly isolated MPE175 cells is shown in Panels B and C. All histograms shown in panels C were gated on CD45 negative/heme-lineage negative (CD14, CD33, GlyA) singlet events with DNA content ≥ 2N as identified in

panels B. The 2N population was determined from the DAPI fluorescence intensity of MPE leukocytes (CD45+CD14+CD33+, blue trace). CD45-CD14-CD33- vimentin+ and cytokeratin+ cells with a DNA profile >2N were classified as aneuploidy tumor cells (green trace). Panels C, From left to right show that a small subset of CD45-CD14-CD33- aneuploidy MPE nucleated cells was double positive for cytokeratin and for vimentin, while the majority of these cells were vimentin + (45%). Even cytokeratin+ tumor cells lost the surface expression of CD326/EpCAM and a small subpopulation expressed surface CD44, CD90 and CD73, known mesenchymal markers, which are significantly upregulated during in vitro tissue culture passage (not shown).

Fig. S3

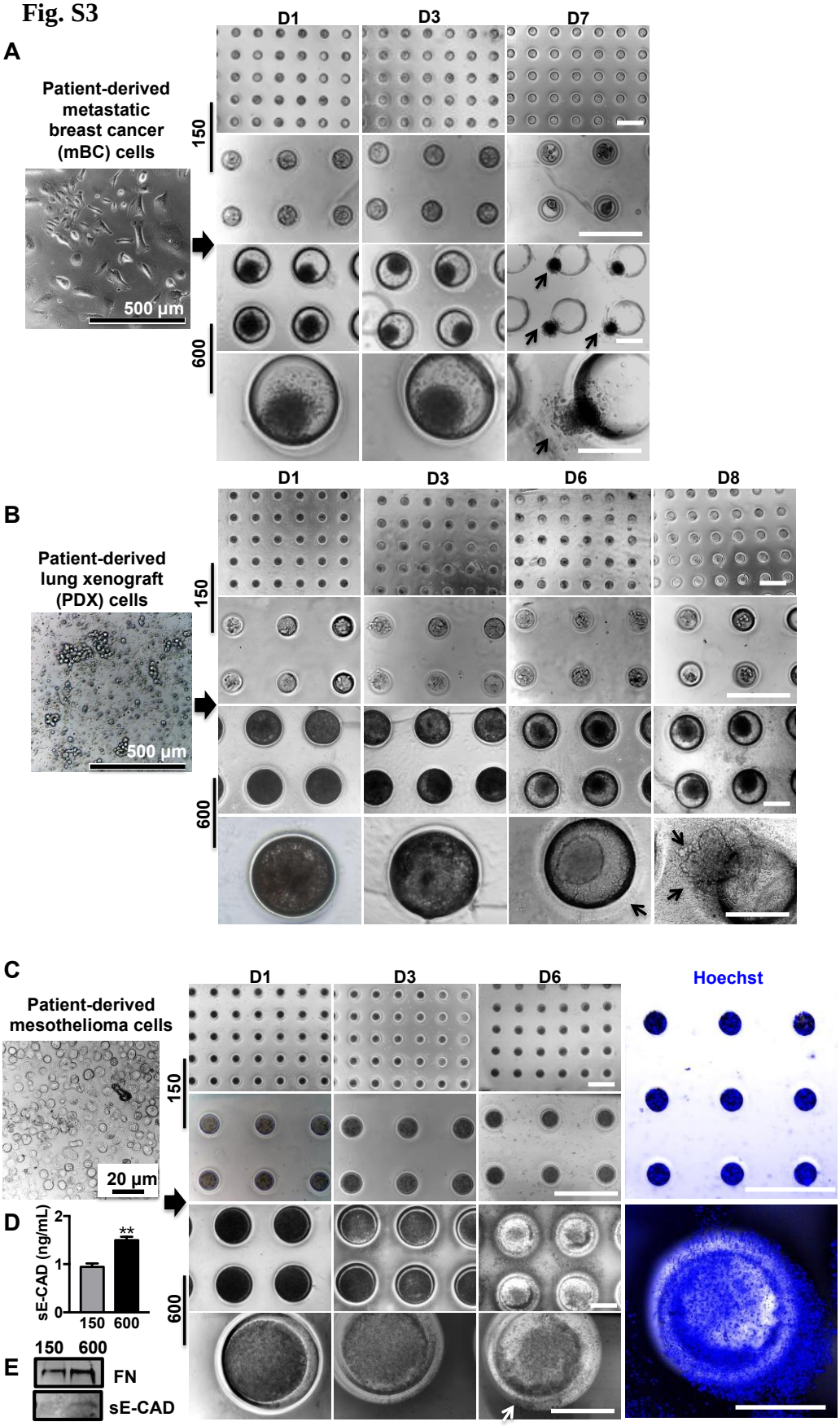
A
Patient-derived metastatic breast cancer (mBC) cells
500 μm
D1
D3
D7
150
600
B
Patient-derived lung xenograft (PDX) cells
500 μm
D1
D3
D6
D8
150
600
C
Patient-derived mesothelioma cells
20 μm
D1
D3
D6
Hoechst
150
600
D
sE-CAD (ng/mL)
2
1
0
**
150
600
E
150
600
FN
sE-CAD

Supplementary Figure S3: Large microtumors of patient-derived primary cancer cells and xenograft cells showed migratory behavior. To validate microenvironment-induced migratory behavior observed in T47D microtumors, patient-derived metastatic breast cancer cells (mBC, n=1 patient tumor), non-small cell lung cancer (NSCLC) derived mouse PDX cells (n=2 tumor samples), and mesothelioma cells (n=1 patient tumor) were seeded on hydrogel microwell arrays (150 and 600 μm). The microtumors were cultured for up to 6-8 days. (A, B) Microtumors from patient-derived mBC cells and PDX cells formed compact microtumors and showed migration in large microtumors. However, we observed much smaller microtumor sizes in the 600 μm microwells. This is due to the differences in the size of the individual cells, which determines the effective seeding density inside the hydrogel microwells and consequently, the size of microtumors. Hence, seeding density needs to be optimized for each cell type in the future studies. We could not do this in the current study due to limitations on the number and size of the patient sample availability; (C) Photomicrographs represent the morphology of mesothelioma cells in 2D (left) and microtumors on hydrogel devices (right). Large mesothelioma microtumors showed similar migratory phenotype that was evident from day 4-6. (D) ELISA results showed higher sE-CAD levels in large microtumors and (E) western blots revealed higher FN and sE-CAD proteins in conditioned media of large microtumors compared to the small ones. Please note that small microtumors (150 μm) in each of the cell type remained non-migratory while large microtumors showed migratory behavior. This also suggests that microtumor size threshold required for migration may differ for different tumor types as well as tumor cell phenotypes. Data presented here for all patient-derived and PDX samples are collected

from at least three 150 and 600 μm hydrogel microwell devices). Scale bar: 500 μm unless mentioned.

Fig. S4

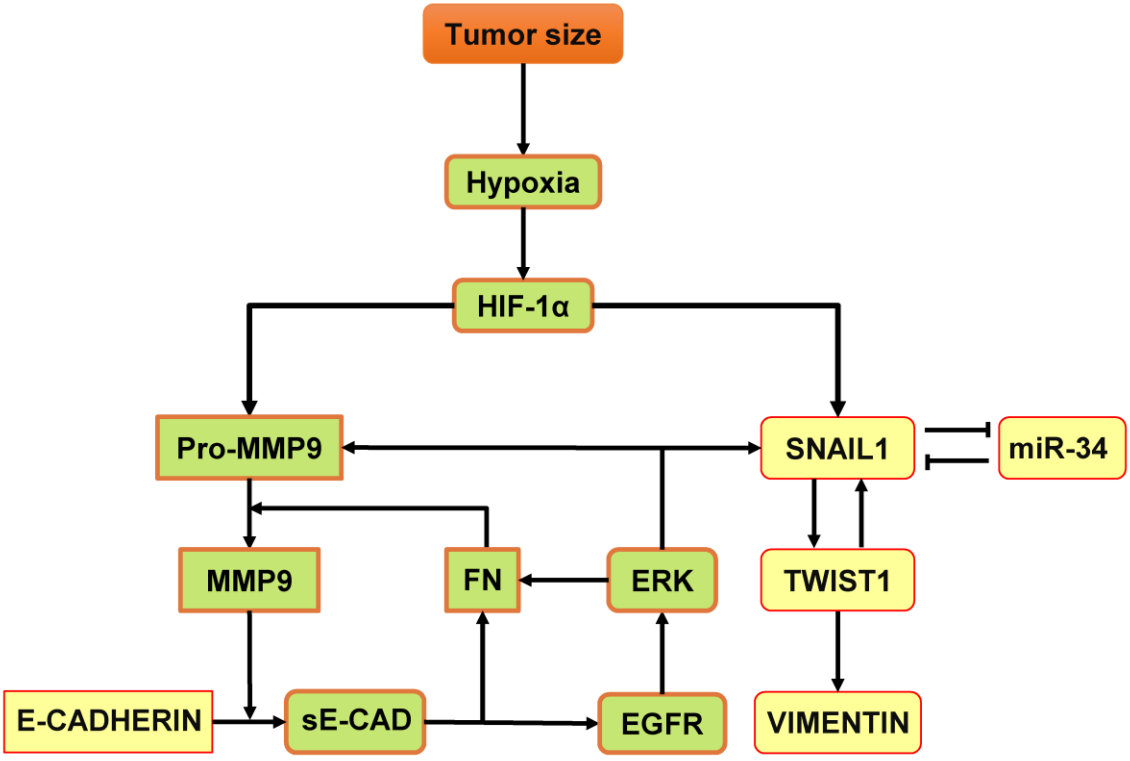

Supplementary Figure S4: Integrated regulatory network of tumor microenvironmental factors and signaling molecules involved in microtumor migration.

Fig. S5

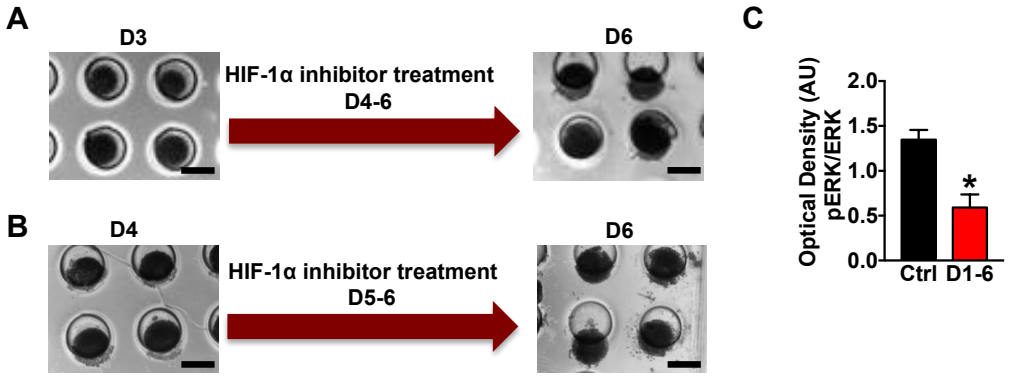

Supplementary Figure S5: HIF-1α inhibition at later time points does not inhibit migration of 600 µm microtumors. To evaluate the effect of inhibition of hypoxia at later time points of culture (Day 4-6 or 5-6), the 600 µm microtumors were treated with 1.0 µM HIF-1α inhibitor on day 4-6 (A) and day 5-6 (B). Photomicrographs revealed that microtumors treated with HIF-1αinhibition on D4-6 and D5-6 continue to migrate. (C) Densitometry of western blot showed > 2.5 fold downregulation of pERK in 600 µm microtumors treated with a HIF-1α inhibitor from Day 1-6. Data represent three independent experiments with three device replicates each containing multiple microtumors. Scale bar: 500 µm.

Fig. S6

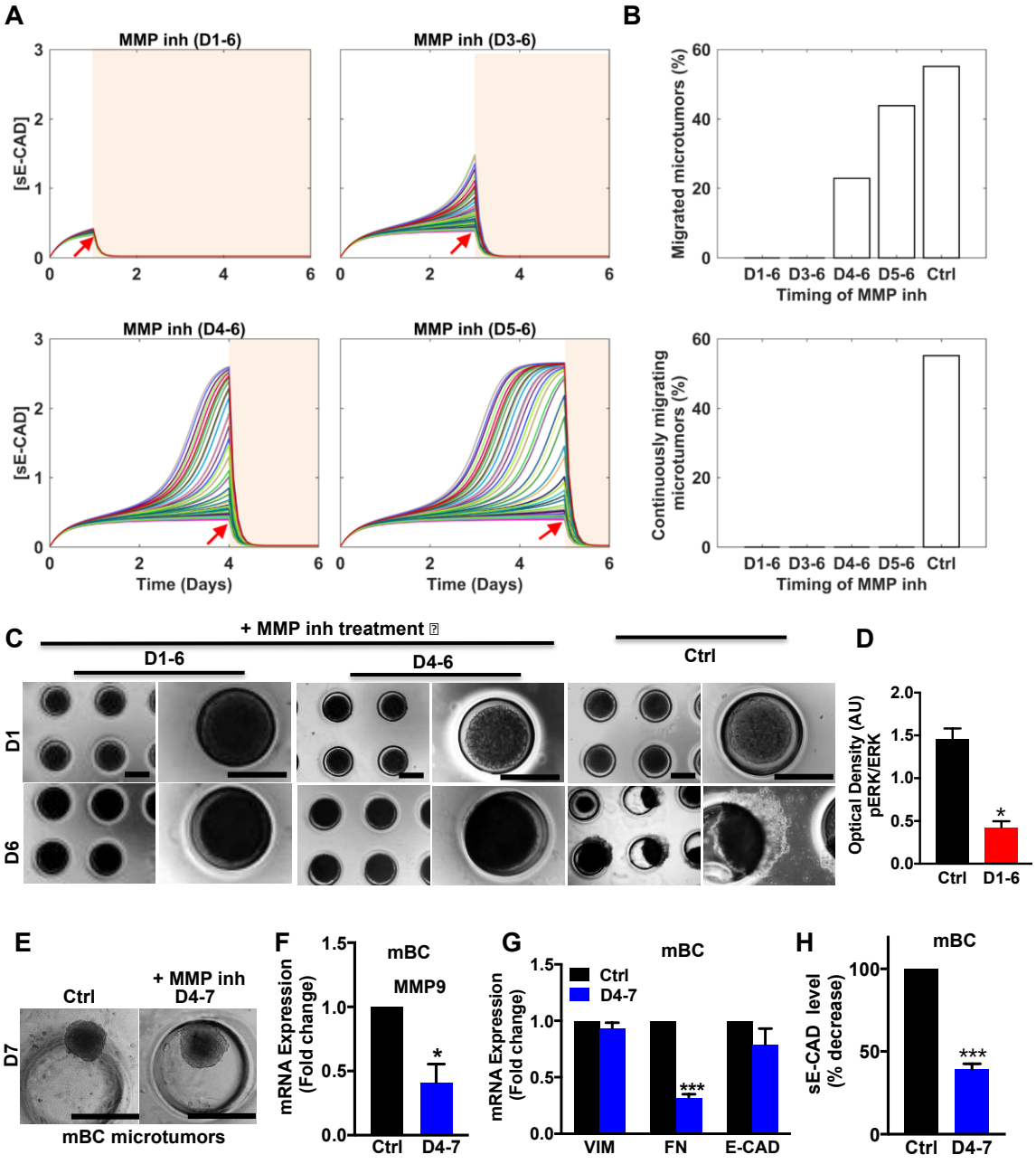

Supplementary Figure S6: Effect of MMP inhibitor treatment on the collective migration of large microtumors of T47D cell line and patient-derived metastatic breast cancer (mBC) cells. (A) The dynamics of sE-CAD for 50 microtumors treated with MMP inhibitor started on day 1, day 3, day 4 and day 5 (red arrows); (B) The fraction of migrated microtumors (upper panel, i) and continuously migrating

microtumors (lower panel, ii) with MMP inhibitor treatment started on day 1, day 3, day 4 and day 5 (sampled with 1000 microtumors); (C) Photomicrographs of 6-day old microtumors treated with MMP inhibitor. GM6001 treatment completely inhibited collective migration in 600 μm T47D microtumors. Scale bar: 500 μm; (D) Densitometry analysis showed downregulation of pERK in GM6001 treated T47D microtumors. (E-H) Effect of MMP inhibitor treatment (day 4-7) in primary patient-derived mBC microtumors; MMP inhibitor treatment inhibited migration (E), downregulated *MMP9* (F) and *FN* mRNA expression without significant effect on *VIM* and *E-CAD* expression (G). (H) MMP inhibition significantly reduced sE-CAD levels in treated microtumors compared to untreated controls. Data are presented as Mean ±SEM. Unpaired t-test was used to analyze significance between control and treated groups. *: $p<0.05$; ***: $p<0.001$ w.r.t. Ctrl (untreated), n=2-3 microwell devices containing multiple microtumors from at least 3 independent experiments for T47D cells (A), and only one experiment for patient-derived mBC microtumors (E-H).

Fig. S7

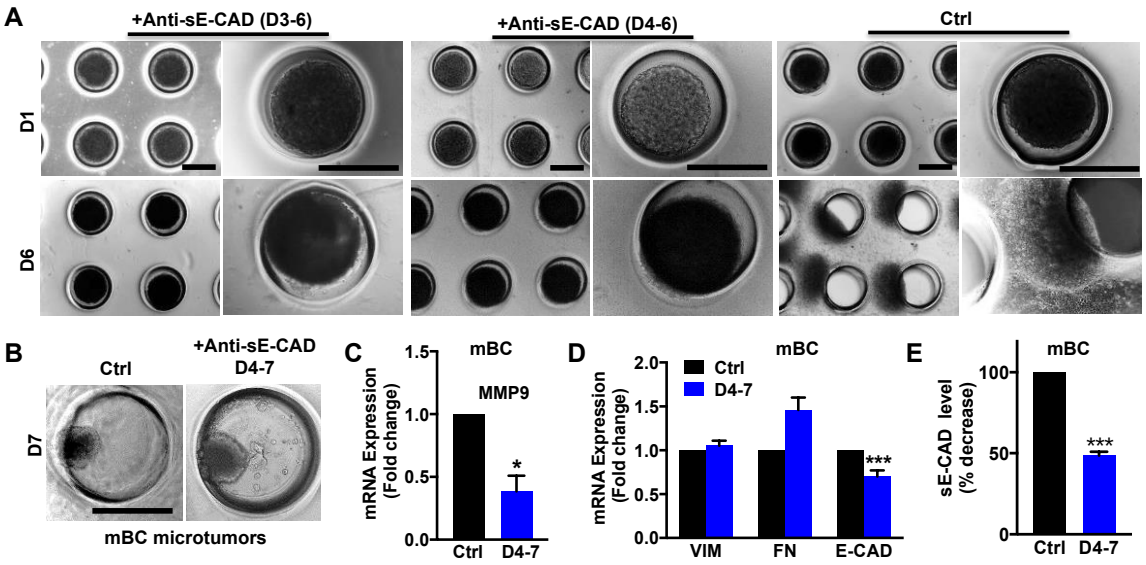

Supplementary Figure S7: (A) Photomicrographs representing day 6 images of anti-sE-CAD antibody-treated T47D microtumors. In contrast to HIF-1α inhibitor treatment, anti-sE-CAD antibody treatment at late time points (day 3-6 and day 4-6) completely inhibited collective migration in 600 μm microtumors. (B) When treated with anti-sE-CAD antibody (40 μg/mL, Day 4-7), large microtumors of primary metastatic breast cancer (mBC) cells showed inhibition of migration and (C) downregulated *MMP9* mRNA expression without significant effect on EMT markers (D). However, anti-sE-CAD antibody treatment significantly reduced sE-CAD levels compared to untreated control. Data are presented as Mean ± SEM. Unpaired t-test was used to analyze significance between control and treated groups. * $p<0.05$; ***$p<0.001$ w.r.t. Ctrl (untreated), n=3 microwell devices containing multiple microtumors from at least 3 independent experiments for T47D cells (A) and only one experiment for patient-derived mBC microtumors (B-D). Scale bar: 500 μm.

References

Brouxhon, S. M., Kyrkanides, S., Teng, X., O'Banion, M. K., Clarke, R., Byers, S., and Ma, L. (2014). Soluble-E-cadherin activates HER and IAP family members in HER2+ and TNBC human breast cancers. Molecular carcinogenesis *53*, 893-906.

Choi, J. Y., Jang, Y. S., Min, S. Y., and Song, J. Y. (2011). Overexpression of MMP-9 and HIF-1α in Breast Cancer Cells under Hypoxic Conditions. Journal of Breast Cancer *14*, 88-95.

Das, S., Banerji, A., Frei, E., and Chatterjee, A. (2008). Rapid expression and activation of MMP-2 and MMP-9 upon exposure of human breast cancer cells (MCF-7) to fibronectin in serum free medium. Life Sciences *82*, 467-476.

De Wever, O., Derycke, L., Hendrix, A., De Meerleer, G., Godeau, F., Depypere, H., and Bracke, M. (2007). Soluble cadherins as cancer biomarkers. Clinical & Experimental Metastasis *24*, 685-697.

Evans, A. J., Russell, R. C., Roche, O., Burry, T. N., Fish, J. E., Chow, V. W. K., Kim, W. Y., Saravanan, A., Maynard, M. A., Gervais, M. L., *et al.* (2007). VHL Promotes E2 Box-Dependent E-Cadherin Transcription by HIF-Mediated Regulation of SIP1 and Snail. Molecular and Cellular Biology *27*, 157-169.

Inge, L. J., Barwe, S. P., D'Ambrosio, J., Gopal, J., Lu, K., Ryazantsev, S., Rajasekaran, S. A., and Rajasekaran, A. K. (2011). Soluble E-cadherin promotes cell survival by activating epidermal growth factor receptor. Experimental cell research *317*, 838-848.

Jeon, M., Lee, J., Nam, S. J., Shin, I., Lee, J. E., and Kim, S. (2015). Induction of fibronectin by HER2 overexpression triggers adhesion and invasion of breast cancer cells. Experimental cell research *333*, 116-126.

Lundgren, K., Nordenskjold, B., and Landberg, G. (2009). Hypoxia, Snail and incomplete epithelial-mesenchymal transition in breast cancer. British journal of cancer *101*, 1769-1781.

Luo, D., Wang, J., Li, J., and Post, M. (2011). Mouse Snail Is a Target Gene for HIF. Molecular Cancer Research *9*, 234-245.

Maretzky, T., Reiss, K., Ludwig, A., Buchholz, J., Scholz, F., Proksch, E., de Strooper, B., Hartmann, D., and Saftig, P. (2005). ADAM10 mediates E-cadherin shedding and regulates epithelial cell-cell adhesion, migration, and β-catenin translocation. Proceedings of the National Academy of Sciences of the United States of America *102*, 9182-9187.

Mitra, A., Chakrabarti, J., Banerji, A., Das, S., and Chatterjee, A. (2006). Culture of human cervical cancer cells, SiHa, in the presence of fibronectin activates MMP-2. Journal of cancer research and clinical oncology *132*, 505-513.

Moshal, K. S., Sen, U., Tyagi, N., Henderson, B., Steed, M., Ovechkin, A. V., and Tyagi, S. C. (2006). Regulation of homocysteine-induced MMP-9 by ERK1/2 pathway. American journal of physiology Cell physiology *290*, C883-891.

Patil, P. U., D'Ambrosio, J., Inge, L. J., Mason, R. W., and Rajasekaran, A. K. (2015). Carcinoma cells induce lumen filling and EMT in epithelial cells through soluble E-cadherin-mediated activation of EGFR. Journal of Cell Science *128*, 4366-4379.

Sen, T., Dutta, A., Maity, G., and Chatterjee, A. (2010). Fibronectin induces matrix metalloproteinase-9 (MMP-9) in human laryngeal carcinoma cells by involving multiple signaling pathways. Biochimie *92*, 1422-1434.

Singh, M., Mukundan, S., Jaramillo, M., Oesterreich, S., and Sant, S. (2016). Three-Dimensional Breast Cancer Models Mimic Hallmarks of Size-Induced Tumor Progression. Cancer research *76*, 3732-3743.

Zhang, L., Huang, G., Li, X., Zhang, Y., Jiang, Y., Shen, J., Liu, J., Wang, Q., Zhu, J., Feng, X., *et al.* (2013). Hypoxia induces epithelial-mesenchymal transition via activation of SNAI1 by hypoxia-inducible factor -1alpha in hepatocellular carcinoma. BMC cancer *13*, 108.

Zuo, J. H., Zhu, W., Li, M. Y., Li, X. H., Yi, H., Zeng, G. Q., Wan, X. X., He, Q. Y., Li, J. H., Qu, J. Q., *et al.* (2011). Activation of EGFR promotes squamous carcinoma SCC10A cell migration and invasion via inducing EMT-like phenotype change and MMP-9-mediated degradation of E-cadherin. J Cell Biochem *112*, 2508-2517.